Evaluation of CLM5.0 for simulating surface energy budget and soil hydrothermal regime in permafrost regions of the Qinghai-Tibet Plateau

Junjie Ma [a,b], Ren Li [a,*], Hongchao Liu [c], Zhongwei Huang [c], Tonghua Wu [a], Xiaodong Wu [a], Lin Zhao [d], Guojie Hu [a], Yao Xiao [a], Yongliang Jiao [a,b], Wenhao Liu [a,b], Shenning Wang [a], Jianzong Shi [a], Yongping Qiao [a]

[a] Cryosphere Research Station on the Qinghai-Tibet Plateau, State Key Laboratory of Cryospheric Science, Northwest Institute of Eco-Environment and Resources, Chinese Academy of Sciences, 320 Donggang West Road, Lanzhou 730000, China
[b] University of Chinese Academy of Sciences, Beijing 100049, China
[c] Key Laboratory for Semi-Arid Climate Change of the Ministry of Education, College of Atmospheric Sciences, Lanzhou University, Lanzhou 730000, China
[d] School of Geographical Sciences, Nanjing University of Information Science & Technology, Nanjing 210044, China

ARTICLE INFO

ABSTRACT

Surface energy budget and soil hydrothermal regime are crucial for understanding the interactions between the atmosphere and land surface. However, large uncertainties in current land surface process models exist, especially for the permafrost regions in the Qinghai-Tibet Plateau. In this study, observed soil temperature, moisture, and surface energy fluxes at four sites in permafrost regions are chosen to evaluate the performance of CLM5.0. Furthermore, the soil property data, different thermal roughness length schemes, and dry surface layer (DSL) scheme are investigated. The results show that the soil property data is important for CLM5.0. The default scheme in CLM5.0 yields large errors for surface energy fluxes. The combination of the thermal roughness length and DSL scheme significantly improved the simulation of surface energy fluxes, especially for latent heat flux. The optimization of DSL scheme significantly improved soil temperature simulation and decreased the *RMSE* from 1.95 °C, 2.07 °C, 2.02 °C, and 2.95 °C to 1.34 °C, 1.35 °C, 1.35 °C and 2.29 °C in TGL site, respectively. The combination of the thermal roughness length and DSL scheme performed the best in shallow soil moisture, decreasing the *RMSE* from 0.136 m³ m⁻³ to 0.049 m³ m⁻³ in the XDT site but slightly enhancing the errors in middle soil. The interactions between surface energy and soil hydrothermal regime also discussed. However, the thermal roughness length and the DSL schemes are highly dependent on the condition of the underlying surface. Different schemes should be selected for different regions.

1. Introduction

The Qinghai-Tibetan Plateau (QTP), which is known as the highest plateau in the world, has been proved to have a significant impact on the Asian summer monsoon and even global climate through its dynamic and thermal effects (Duan et al., 2012; Wu et al., 2012; Xin et al., 2018). The underlying surface of the QTP is complex and has extensive permafrost distribution (Zou et al., 2017). In permafrost regions, the diurnal variation of surface energy fluxes and near-surface meteorological elements is drastic, which have significant impacts on regional and global climate change (Ma et al., 2004; Yao et al., 2019). Permafrost is also sensitive to climate change, the surface air temperature on the QTP has increased at 0.40–0.52 °C per decade since the 1980s and this

has resulted in substantial degradation of the permafrost (Cheng and Wu, 2007; Cheng et al., 2019; Zhao et al., 2020), which may in turn release more greenhouse gasses into the atmosphere (Mu et al., 2020). Thus, the interactions between the land surface and atmosphere in QTP plays an essential role in understanding the climate change (Luo et al., 2017; Ma et al., 2022a; Zhang et al., 2011).

Due to its remote location, there are rare observation sites in QTP (Cao et al., 2019; Deng et al., 2020). Compared to the *in-situ* observations and reanalysis data, land surface process models (LSMs) provide a more convenient way for the land surface process researches and the future forecast (Ma et al., 2022b). The realistically simulations of the complex interactions between the land surface and the atmosphere are significant, however, numerous studies reveals that many LSMs have

difficulties in reliably simulating the land surface processes, such as the surface energy fluxes, soil temperature and moisture, the snow cover process (Gao et al., 2016; Li et al., 2020; Ma et al., 2008; Yang et al., 2009; Zhang et al., 2016).

Many modifications have been made to improve the simulation effect of the surface energy budget and soil hydrothermal regime in LSMs. The thermal roughness length (z_{0h}) is an important parameter for calculating sensible heat flux (H) in both LSMs and climate models. Moreover, several theoretical and experimental z_{0h} schemes have been proposed recently. Yang et al. (2003) developed a z_{0h} scheme based on the wind and temperature profiles; the H can be calculated more accurately in combination with aerodynamic methods. Zeng et al. (2012) modified the coefficients in the default z_{0h} scheme of CLM4.5, and improved the simulation effect of H. Furthermore, changes in z_{0h} can also affect the characteristics of other parameters, such as soil temperatures (Li et al., 2021). Chen et al. (2011) adjusted the z_{0h} scheme in Noah; they found that the soil temperature was also ameliorated. The soil evaporation resistance is also a crucial parameter for surface evaporation and soil moisture (Yang et al., 2009). Results showed that the modification in the soil evaporation resistance could effectively reduce the overestimation of soil moisture on the QTP (Deng et al., 2021). Numerous studies have proven that the simulation results can be improved by replacing appropriate parameterization schemes in LSMs (Chen et al., 2013; Wang et al., 2019b; Yang et al., 2009; Zhang et al., 2021a). However, most of these studies focused on soil temperature and moisture simulations in seasonally frozen ground soils (Deng et al., 2020, 2021). Only a few studies considered the evaluation and improvement of the surface energy fluxes in the permafrost regions (Wang and Ma, 2019). Therefore, further studies on the performance for surface energy fluxes of the LSMs in permafrost regions are still necessary.

The Community Land Model (CLM) is the land surface module in the Community Earth System Model (CESM). It is one of the most developed and potential LSMs in the world (Dickinson et al., 2006). The latest version, CLM5.0, has made great progress in the key parameters compared to its previous version (Deng et al., 2020; Lawrence et al., 2019). This study used CLM5.0 to conduct the simulation of the surface energy budget and soil hydrothermal regime in permafrost regions of the QTP. We primarily aim to investigate the impact of different thermal roughness length and dry surface layer schemes on the simulation results of surface energy fluxes and the interactions between surface energy budget and soil hydrothermal regime. The paper is organized as follows: Section 2 describes the study area and method. The model description and experiment designs are introduced in Section 3. Section 4 presents the simulation results for the soil temperature, moisture, and surface energy fluxes of different experiments. Section 5 discusses the key processes associated with soil hydrothermal and surface energy budget regimes. Section 6 presents conclusions.

2. Study area and methods

2.1. Study area and in-situ observation

This study chose the following four typical underlying surface monitoring sites in permafrost regions over the QTP: Beiluhe station (BLH), Liangdaohe station (LDH), Tanggula station (TGL), and Xidatan station (XDT) (Fig. 1). The BLH station is located between Hoh Xil and Fenghuoshan on the central QTP. The TGL station is situated southwest of Tanggula Mountain on the hinterland of the QTP; It is the highest altitude observation station in the permafrost area. Furthermore, XDT is located along the boundary of permafrost in the northern QTP, representing the characteristics of the island-shaped permafrost. The LDH station has the lowest latitude, the warmest climate, and the most abundant precipitation (Zhao et al., 2021). The XDT and LDH stations extend from close to the northernmost (XDT) to the southernmost (LDH) of permafrost. Table 1 provides the details about the four monitoring sites.

The atmospheric forcing data required by the CLM5.0 offline simulation included the following: surface air temperature, precipitation, wind speed, pressure, downward shortwave radiation, specific humidity, and upward longwave radiation. Furthermore, Table 1 lists the time resolution of each station. The precipitation data at the LDH station had a large error during the selected period due to harsh natural conditions. We extracted the closest points from the China Meteorological Forcing Dataset (CMFD) to replace the precipitation data The accuracy of the CMFD dataset has been acknowledged; it has been widely used in LSMs over the QTP (Deng et al., 2020; Zhang et al., 2021b).

Additionally, observed soil temperature and soil moisture at different soil depths and surface energy fluxes (including H, latent heat flux (LE), net radiation flux (R_n), and ground heat flux (G_0)) at the four stations were collected to verify the simulation performance of CLM5.0. The soil temperature was measured using a 105T/109 thermocouple probe (Campbell Scientific, Inc., USA) with an accuracy of 0.1 °C/0.2 °C. Furthermore, a Stevens hydro probe (Stevens Water Monitoring System, Inc., USA) with ± 3% accuracy was used to obtain the soil moisture content from 2 to 320 cm below the ground. Among four stations, only TGL and XDT stations have the eddy covariance system. A 3D ultrasonic anemometer and an open-path infrared gas analyzer are involved in the eddy covariance system. Yao et al. (2020) provided a detailed description of calculating H and LE. Moreover, please refer to Ma et al. (2022a) for the description of the calculation method of R_n and G_0.
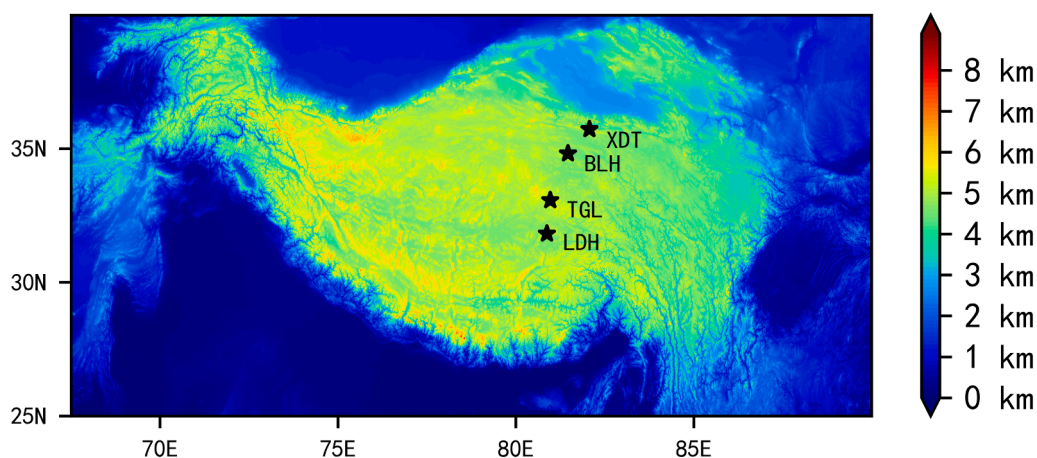
Fig. 1. Locations of the monitoring sites in this study over the QTP.

Table 1
Information of *in-situ* monitoring sites used in this study.

Station	Lon (°E)	Lat (°N)	Land cover type	Altitude (m)	Time resolution	Study period
BLH	92.92	34.82	Alpine swamp	4656	1 h	2009.8.1–2010.7.31
LDH	91.74	31.82	Alpine wet meadow	4808	10 min	2017.1.1–2017.12.31
TGL	91.93	33.07	Alpine grassy meadow	5100	30 min	2006.8.1–2007.7.31
XDT	94.13	35.72	Alpine meadow	4538	30 min	2013.8.1–2014.7.31

2.2. Methods

The performance of CLM5.0 was evaluated based on the simulated and observed values. This study selected the correlation coefficient (*R*), root mean square error (*RMSE*), mean bias error (*MBE*), and mean absolute error (*MAE*) to evaluate the simulation performance of the models in different experiments. Their formulas are as follows:

$$R = \frac{\sum_{i=1}^{N}(M_i - \overline{M})(O_i - \overline{O})}{\sqrt{\sum_{i=1}^{N}(M_i - \overline{M})^2} \cdot \sqrt{\sum_{i=1}^{N}(O_i - \overline{O})^2}}, \tag{1}$$

$$RMSE = \sqrt{\frac{1}{N}\left(\sum_{i=1}^{N}(M_i - O_i)^2\right)}, \tag{2}$$

$$MBE = \frac{1}{N}\sum_{i=1}^{N}(M_i - O_i), \tag{3}$$

$$MAE = \frac{1}{N}\sum_{i=1}^{N}|(M_i - O_i)|, \tag{4}$$

where M_i and O_i correspond to the simulated and observed values, respectively; M and O denote the average of simulated and observed values, respectively; N is the length of the study time series.

3. Model

3.1. Model description

CLM5.0 is the latest generation land surface process model released by NCAR (National Center for Atmosphere Research). It provides a detailed description of land surface processes, including biogeophysical, biogeochemical, dynamic vegetation, and water cycle processes. Compared with prior CLM versions, some novel parameterizations or model structural decisions have been updated in CLM5.0, mainly including soil hydrology, surface turbulent flux, snow cover, vegetation physiology, carbon and nutrient dynamics, and river modeling (Lawrence et al., 2019). CLM5.0 introduces the soil evaporation resistance parameterization scheme of dry surface layer (DSL), improving the simulation of soil evaporation (Swenson and Lawrence, 2014). These improvements make CLM5.0 more accurate in simulating soil water and heat transfer processes and surface energy flux (Deng et al., 2020, 2021; Luo et al., 2020).

3.2. Model setup

This study performed single-point offline simulations at four observation stations of the permafrost regions over the QTP using CLM5.0. We selected the "I" compset and ran the satellite phenology model (CLMSP). For each experiment, a one-month simulation was used for spin-up. This study selected two consecutive years with better data quality and simulated it from August of the first year to July of the next year to eliminate the error of the initial ice content to analyze a complete freeze-thaw cycle process. The simulation was started in January because the data at the LDH site was only measured for one year.

3.3. Thermal roughness length scheme

The sensible heat flux in CLM5.0 is based on the Monin-Obukhov similarity theory. It was calculated as shown in Eq. (5):

$$H = \rho_{atm}C_p\frac{(T_s - T_a)}{r_{ah}}, \tag{5}$$

where ρ_{atm} denotes the density of atmospheric air (kg m^{-3}), and C_p corresponds to the specific heat capacity of air (J kg^{-1} K^{-1}); T_a and T_s denote the air temperature (K) and surface ground temperature (K), respectively. Moreover, r_{ah} is the aerodynamic resistance (s m^{-1}), which was calculated using Eq. (6),

$$r_{ah} = \frac{1}{k^2 V_a}\left[\ln\frac{z-d}{z_{0m}} - \psi_m\left(\frac{z-d}{L}\right) + \psi_m\left(\frac{z_{0m}}{L}\right)\right]\left[\ln\frac{z-d}{z_{0h}} - \psi_h\left(\frac{z-d}{L}\right) + \psi_h\left(\frac{z_{0h}}{L}\right)\right], \tag{6}$$

where L represents the Monin-Obukhov length, z_{0m} and z_{0h} denote the momentum and thermal roughness length, respectively; z_{0m} is the height at which the average wind speed is equal to zero, and z_{0h} represents the height at which the air temperature is equal to the surface ground temperature; z is the height above the surface, d denotes the zero plane displacement height, ψ_h and ψ_m correspond to the stability correction functions, and k denotes von Karman's constant, which was set to 0.4.

In CLM5.0, the default scalar roughness height for sensible heat transfer was derived following Zeng and Dickinson (1998):

$$z_{0h} = z_{0m}e^{-a(u_* z_{0m}/v)^{0.45}}, \tag{7}$$

where the quantity $u_* z_{0m}/v$ corresponds to the roughness Reynolds number (R_{e*}), the kinematic viscosity of air was $v = 1.5 \times 10^{-5}$ m^2 s^{-1} and $a = 0.13$.

The z_{0h} parameterization scheme is a crucial parameter in estimating sensible heat flux, which also has an important impact on the surface energy budget and soil water and heat transfer (Chen et al., 2013; Li et al., 2020). The default scheme of CLM5.0 is mainly applicable to bare land and snow covered surface. Some studies show that this scheme is overestimated in the sensible heat flux simulation of the QTP (Wang et al., 2019b), and we have similar conclusions in the permafrost region of the QTP. It is very effective to select appropriate thermal roughness length scheme for different types of underlying surfaces to improve energy flux simulation. Herein, we incorporated two other widely used thermal roughness length schemes—Brutsaert (1982) (B82) and Yang et al. (2008) (Y08) schemes—into CLM5.0 to determine the effects of the thermal roughness length scheme on surface energy flux and soil water and heat transfer. B82 scheme is suitable for rough rigid surface, high vegetation and forest surface. Studies have shown that B82 scheme can improve the overestimation of CLM in sensible heat simulation over the QTP (Wu et al., 2022). The Y08 scheme is mainly designed for the sparse, low and short grass in the QTP, which is more suitable for the simulation of energy flux in the QTP (Li et al., 2020).

In the B82 scheme, the thermal roughness length depends on the R_{e*}, which was calculated by Eq. (8),

$$z_{0h} = z_{0m}\exp(2.0 - 2.46R_{e*}^{0.25}), \tag{8}$$

The Y08 scheme has been widely used in land surface models, it can simulate an evident diurnal variation of z_{0h} (Chen et al., 2011). This

scheme is defined as

$$z_{0h} = (70v \, / \, u_*) \exp\left(-\beta u_*^{0.5}|T_*|^{0.25}\right),\tag{9}$$

where $\beta = 7.2 \, m^{-\frac{1}{2}}s^{\frac{1}{2}}k^{-\frac{1}{4}}$, and v is the kinematic viscosity of air.

3.4. Dry surface layer scheme

Compared with CLM4.5, CLM5.0 has introduced the evapotranspiration soil resistance scheme based on the thickness of the dry soil layer, improving the simulation accuracy of evapotranspiration in semi-arid areas to a certain extent (Swenson and Lawrence, 2014). The soil evaporation scheme in CLM5.0 is as follows:

$$E_{soil} = -\frac{\rho_{atm}(q_{atm} - q_{soil})}{r_{aw} + r_{soil}},\tag{10}$$

where q_{atm} and q_{soil} correspond to the atmospheric specific humidity (kg^{-1}) and specific humidity (kg^{-1}) of the soil, respectively; r_{aw} denotes the aerodynamic resistance to water vapor transfer (s m^{-1}); r_{soi} represents the soil resistance to water vapor transfer (s m^{-1}), which is a crucial parameter for calculating the surface evaporation and soil moisture within the topsoil (Yang et al., 2009). It was calculated using Eq. (11),

$$r_{soil} = \frac{DSL}{D_v \tau},\tag{11}$$

where DSL (m) is the dry surface layer thickness, D_v denotes the molecular diffusivity of atmospheric water vapor ($m^2 \, s^{-2}$), and τ represents the tortuosity of the vapor flow paths through the soil matrix (Swenson and Lawrence, 2014).

The DSL in CLM5.0 is given by

$$DSL = \begin{cases} \Delta z \dfrac{\theta_{dsl0} - \theta_{top}}{\theta_{dsl0} - \theta_{air}}, \theta_{top} < \theta_{dsl0} \\ 0, \ \theta_{top} \geq \theta_{dsl0} \end{cases},\tag{12}$$

where Δz describes the length scale of the maximum DSL thickness (default value was 15 mm); θ_{dsl0} ($mm^3 \, mm^{-3}$), θ_{top} ($mm^3 \, mm^{-3}$), and θ_{air} ($mm^3 \, mm^{-3}$) denote the moisture values of the DSL initiates, top soil layer, and the "air dry" soil, respectively.

$$\theta_{dsl0} = k\Phi,\tag{13}$$

where Φ denotes the porosity, and $k = 0.8$, which is calibrated by comparing the simulation performance at reproducing the Gravity Recovery and Climate Experiment satellite project total water storage seasonal characteristics globally (Swenson and Lawrence, 2014).

DSL scheme in CLM5.0 is primarily aimed at improving the accuracy of evapotranspiration simulations in semi-arid regions around the world. However, due to the complexity of the underlying surface of the QTP, the soil texture in permafrost regions remain large difference from other region, the performance of the default k value in the permafrost region of the QTP may not ideal. The surface soil moisture in TGL site is approximately 0.2 $m^3 \, m^{-3}$ during thawing stage, and the porosity of top soil is about 0.55. When $k = 0.8$, θ_{dsl0} is 0.44 $m^3 \, m^{-3}$, which is significantly higher than the annual soil moisture of TGL site. Furthermore, a recent study showed that the DSL scheme in CLM5.0 might result in the overestimation of soil moisture over the QTP (Deng et al., 2020), which may cause the underestimation of latent heat flux. Herein, in this study, we set the value of $k = 0.4$, which is calibrated via the observation results of soil moisture and soil particle size in the permafrost regions of the QTP.

3.5. Experimental designs

This study designed sensitivity experiments (SP1, SP2, SP3, SP4, SP5, and SP6) and one control experiment (CTL) to investigate the influence of soil property data, thermal roughness length scheme, and soil resistance scheme on soil water and heat transfer and surface energy fluxes. Table 2 provides details of the designs of experiments by CLM5.0. The CLM5.0 default scheme and soil property data were used in the CTL experiment. However, the observed surface data (including percent of clay, sand, and soil organic matter) in the sensitivity experiments (SP1, SP2, SP3, SP4, SP5, and SP6) were used.

4. Results

4.1. Soil temperature

Fig. 2 shows the comparison of daily mean soil temperature between observation and simulation at four soil depths (10 cm, 50 cm, 80 cm, and 210 cm) in the four stations (TGL, BLH, XDT, and LDH). CLM5.0 can better reflect the seasonal pattern of the soil temperature at the four sites; the simulation effect of shallow soil temperature was better than that of deep soil. The simulation performance of the CLM5.0 model at different stations was slightly different. Out of the four stations, the simulation effect of TGL and BLH was found to be better than that of XDT and LDH. Table 3 shows the statistics between different experiments.

The best simulation results were obtained with the DSL parameterized scheme (SP4, SP5, and SP6) for different scheme experiments (CTL test and SP1-SP6). SP4 test decreased the *RMSE* of the four depth soil temperatures from 1.95 °C, 2.07 °C, 2.02 °C, and 2.95 °C to 1.34 °C, 1.35 °C, 1.35 °C, and 2.29 °C, respectively, for the TGL station compared to the CTL test. The tests with the highest correlation coefficients were SP5 and SP6, with four soil layers of 0.99, 0.98, 0.98, and 0.94, respectively. Furthermore, the SP4 test also showed the best agreement with observation in *MAE*; its values decreased from 1.65 °C, 1.72 °C, 1.65 °C, and 2.49 °C to 1.02 °C, 1.05 °C, 1.07 °C, and 1.95 °C, respectively. SP5 showed the best performance for the *MBE* in the shallow soil (10 cm); the value decreased from 0.87 °C to 0.11 °C, i.e., 87% reduction, for middle and deep soils (50 cm, 80 cm, and 210 cm). Moreover, SP4 showed the best performance, reducing the value from 0.99 °C, 0.91 °C, and 1.16 °C to 0.23 °C (77%), 0.27 °C (70%), and 0.68 °C (41%), respectively. The other three stations also had a similar phenomenon.

4.2. Soil moisture

Modeled soil moisture was evaluated with the observed values. Fig. 3 compares the simulated and observed daily mean of soil moisture at three stations (TGL, BLH, and XDT). CLM5.0 captured well the temporal pattern of the soil moisture at the three stations. CLM5.0 had overestimated in the thawed stage and underestimated in the frozen stage in the TGL and BLH stations for the shallow soil; Overestimation in the entire period for the XDT station was noted. The TGL station underestimated the middle and deep soil. An overestimation was observed for the BLH and XDT stations in the middle and deep soil. Table 4 shows the statistics of soil moisture at the three stations between different experiments.

SP5 showed a significant improvement compared to the CTL test in

Table 2
Designs of experiments by CLM5.0.

Experiment name	Soil property data	Thermal roughness length scheme	Soil resistance scheme
CTL	Default	Default	Default
SP1	Observation	Default	Default
SP2	Observation	Y08	Default
SP3	Observation	B82	Default
SP4	Observation	Default	Modified
SP5	Observation	Y08	Modified
SP6	Observation	B82	Modified
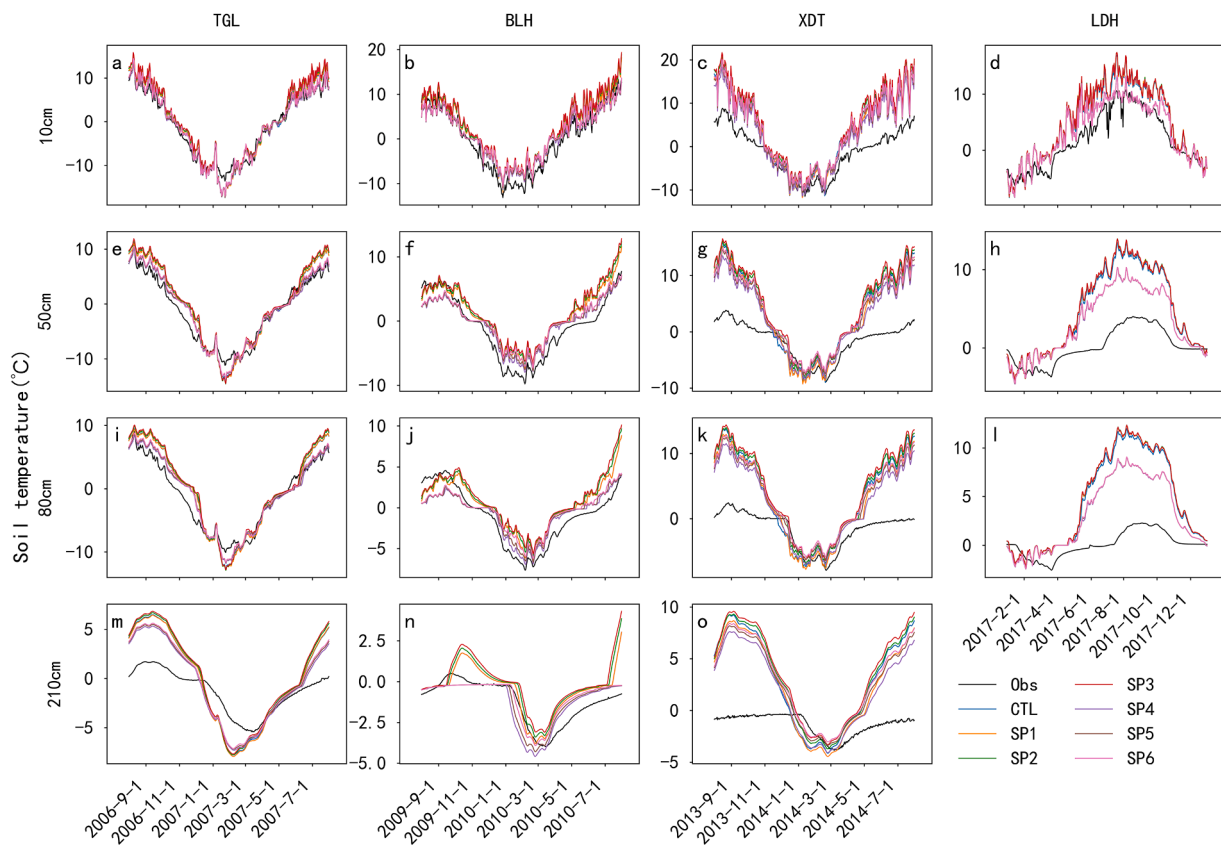
Fig. 2. Comparison of daily mean observed and simulated soil temperature (°C) at the four stations.

Table 3
Statistical results between the simulated and observed soil temperatures at the four stations.

Experiment	Station Soil depth	TGL 10cm	50cm	80cm	210cm	BLH 10cm	50cm	80cm	210cm	XDT 10cm	50cm	80cm	210cm	LDH 10cm	50cm	80cm
CTL	RMSE	1.95	2.07	2.02	2.95	2.68	2.31	1.98	1.02	6.40	6.78	6.62	5.66	3.82	5.52	5.71
	R	0.99	0.98	0.97	0.94	0.98	0.96	0.92	0.86	0.96	0.90	0.85	0.66	0.95	0.88	0.82
	MAE	1.65	1.72	1.65	2.49	2.36	2.05	1.79	0.79	5.27	5.51	5.36	4.64	3.22	4.51	4.50
	MBE	0.87	0.99	0.91	1.16	2.22	1.89	1.45	0.72	5.18	5.02	4.86	4.14	3.04	4.33	4.35
SP1	RMSE	2.00	2.11	2.04	2.96	2.67	2.30	1.97	1.01	5.97	6.25	6.09	5.27	4.02	5.74	5.93
	R	0.99	0.98	0.97	0.94	0.98	0.96	0.92	0.87	0.97	0.92	0.87	0.70	0.95	0.88	0.82
	MAE	1.68	1.75	1.66	2.52	2.34	2.05	1.78	0.79	4.84	4.96	4.83	4.32	3.40	4.69	4.67
	MBE	0.86	0.95	0.88	1.12	2.22	1.87	1.42	0.71	4.76	4.52	4.35	3.72	3.23	4.51	4.53
SP2	RMSE	2.23	2.31	2.22	3.08	3.04	2.65	2.31	1.24	7.04	7.12	6.89	5.88	4.05	5.77	5.95
	R	0.99	0.98	0.97	0.93	0.98	0.96	0.90	0.83	0.97	0.92	0.88	0.71	0.95	0.88	0.82
	MAE	1.91	1.92	1.82	2.59	2.72	2.36	2.04	0.98	5.92	5.74	5.50	4.81	3.42	4.71	4.69
	MBE	1.18	1.25	1.16	1.35	2.65	2.23	1.75	0.94	5.91	5.58	5.36	4.54	3.25	4.53	4.55
SP3	RMSE	2.40	2.47	2.35	3.15	3.30	2.89	2.54	1.43	7.51	7.51	7.25	6.16	4.05	5.76	5.95
	R	0.98	0.98	0.97	0.93	0.98	0.96	0.89	0.81	0.97	0.92	0.88	0.72	0.95	0.88	0.82
	MAE	2.07	2.06	1.95	2.64	2.99	2.58	2.23	1.15	6.44	6.14	5.87	5.05	3.42	4.71	4.70
	MBE	1.40	1.46	1.36	1.52	2.95	2.49	1.99	1.12	6.44	6.08	5.84	4.92	3.25	4.53	4.55
SP4	RMSE	1.34	1.35	1.35	2.29	1.99	1.67	1.41	0.76	5.18	5.37	5.22	4.62	2.41	3.81	4.04
	R	0.99	0.98	0.97	0.94	0.98	0.97	0.93	0.85	0.97	0.92	0.88	0.72	0.93	0.88	0.81
	MAE	1.02	1.07	1.05	1.93	1.70	1.47	1.21	0.59	4.19	4.30	4.16	3.76	1.84	3.17	3.23
	MBE	−0.12	0.23	0.27	0.68	0.74	0.57	0.27	−0.01	4.07	3.96	3.82	3.29	1.51	2.93	3.01
SP5	RMSE	1.37	1.41	1.40	2.36	2.15	1.83	1.53	0.68	6.03	6.05	5.84	5.08	2.43	3.83	4.06
	R	0.99	0.98	0.98	0.94	0.98	0.97	0.93	0.87	0.96	0.92	0.88	0.72	0.93	0.88	0.81
	MAE	1.06	1.13	1.08	1.99	1.84	1.62	1.36	0.55	5.03	4.93	4.74	4.15	1.85	3.19	3.24
	MBE	0.11	0.44	0.47	0.85	1.00	0.79	0.46	0.12	5.02	4.81	4.63	3.95	1.53	2.96	3.04
SP6	RMSE	1.36	1.43	1.42	2.43	2.32	2.02	1.69	0.66	6.44	6.41	6.16	5.33	2.44	3.84	4.07
	R	0.99	0.98	0.98	0.94	0.98	0.96	0.92	0.88	0.96	0.92	0.88	0.72	0.93	0.88	0.81
	MAE	1.07	1.17	1.10	2.06	1.98	1.76	1.52	0.52	5.49	5.30	5.07	4.40	1.86	3.20	3.25
	MBE	0.24	0.56	0.58	0.94	1.28	1.03	0.67	0.26	5.49	5.24	5.03	4.28	1.54	2.97	3.05

the shallow soil (5 cm) at the three stations. For example, the *RMSE* decreased from 0.045 m^3 m^{-3} to 0.035 m^3 m^{-3} in TGL station, from 0.089 m^3 m^{-3} to 0.055 m^3 m^{-3} in BLH station, and from 0.136 m^3 m^{-3} to 0.049 m^3 m^{-3} in XDT station. The *R-value* of the three stations also improved effectively, from 0.88, 0.86, and 0.76 to 0.92, 0.92, and 0.85, respectively. Overestimation for the thawed period at the three stations
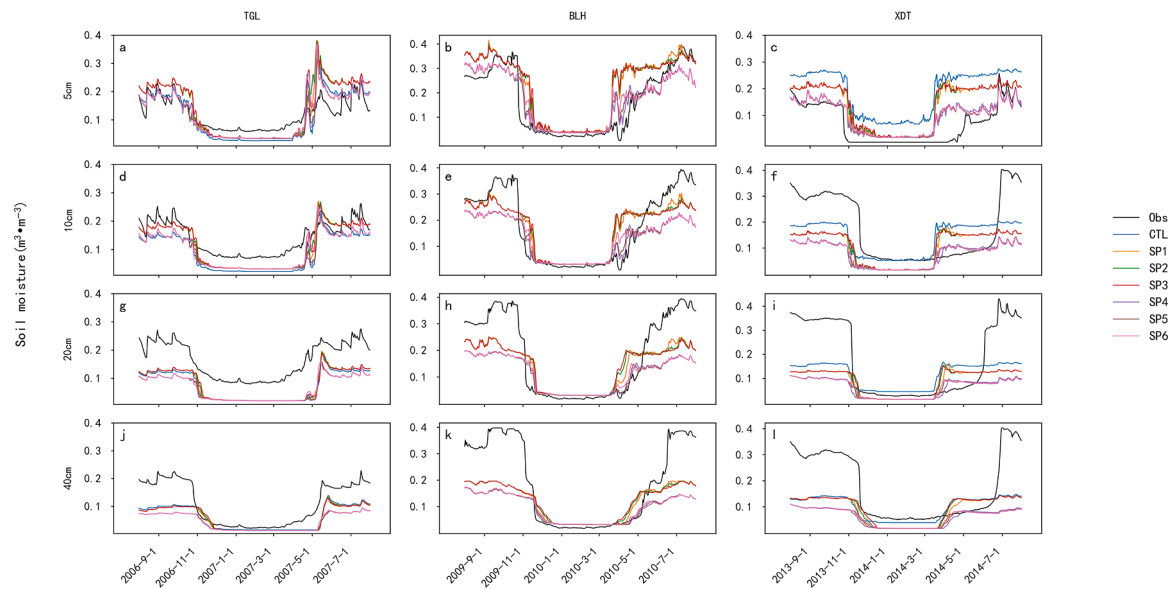
Fig. 3. Comparison of daily mean of observed and simulated soil moisture ($m^3 \, m^{-3}$) at the three stations.

Table 4
Statistical results between the simulated and observed soil moisture at the three stations.

Experiment	Soil depth	TGL				BLH				XDT			
		5cm	10cm	20cm	40cm	5cm	10cm	20cm	40cm	5cm	10cm	20cm	40cm
CTL	*RMSE*	0.045	0.057	0.095	0.062	0.089	0.071	0.092	0.117	0.134	0.108	0.133	0.123
	R	0.88	0.92	0.90	0.92	0.86	0.87	0.90	0.91	0.76	0.58	0.74	0.73
	MAE	0.037	0.052	0.090	0.049	0.062	0.051	0.073	0.083	0.123	0.086	0.105	0.091
	MBE	−0.004	−0.051	−0.090	−0.048	0.057	−0.006	−0.041	−0.066	0.123	−0.031	−0.060	−0.074
SP1	*RMSE*	0.059	0.043	0.091	0.065	0.088	0.070	0.091	0.116	0.091	0.125	0.149	0.126
	R	0.88	0.92	0.91	0.92	0.87	0.87	0.90	0.93	0.75	0.56	0.74	0.76
	MAE	0.047	0.037	0.087	0.052	0.061	0.051	0.072	0.083	0.071	0.104	0.113	0.098
	MBE	0.019	−0.028	−0.087	−0.051	0.056	−0.005	−0.041	−0.066	0.071	−0.068	−0.090	−0.085
SP2	*RMSE*	0.059	0.041	0.091	0.065	0.091	0.075	0.096	0.118	0.094	0.122	0.149	0.125
	R	0.89	0.92	0.91	0.91	0.85	0.85	0.87	0.91	0.74	0.58	0.71	0.73
	MAE	0.048	0.036	0.087	0.052	0.062	0.055	0.077	0.086	0.074	0.102	0.113	0.097
	MBE	0.021	−0.027	−0.087	−0.051	0.056	−0.005	−0.040	−0.065	0.073	−0.066	−0.088	−0.082
SP3	*RMSE*	0.057	0.040	0.091	0.066	0.094	0.077	0.098	0.119	0.095	0.121	0.149	0.125
	R	0.89	0.93	0.91	0.91	0.84	0.84	0.86	0.91	0.73	0.59	0.71	0.72
	MAE	0.046	0.036	0.086	0.053	0.063	0.057	0.079	0.088	0.075	0.102	0.113	0.096
	MBE	0.020	−0.027	−0.086	−0.051	0.057	−0.004	−0.039	−0.064	0.075	−0.065	−0.087	−0.080
SP4	*RMSE*	0.036	0.051	0.104	0.079	0.052	0.081	0.116	0.141	0.049	0.139	0.167	0.150
	R	0.91	0.92	0.91	0.95	0.93	0.94	0.93	0.95	0.86	0.68	0.81	0.80
	MAE	0.029	0.047	0.099	0.063	0.038	0.059	0.086	0.100	0.036	0.104	0.120	0.112
	MBE	−0.006	−0.046	−0.099	−0.063	0.003	−0.043	−0.071	−0.092	0.031	−0.096	−0.113	−0.112
SP5	*RMSE*	0.035	0.050	0.104	0.080	0.055	0.082	0.116	0.141	0.049	0.139	0.168	0.151
	R	0.92	0.93	0.91	0.95	0.92	0.92	0.92	0.95	0.85	0.69	0.80	0.79
	MAE	0.028	0.046	0.099	0.063	0.041	0.062	0.086	0.100	0.036	0.104	0.120	0.111
	MBE	−0.005	−0.045	−0.099	−0.063	0.005	−0.041	−0.070	−0.090	0.030	−0.096	−0.113	−0.111
SP6	*RMSE*	0.039	0.047	0.102	0.079	0.061	0.084	0.116	0.140	0.050	0.138	0.168	0.151
	R	0.89	0.94	0.93	0.95	0.90	0.90	0.91	0.94	0.84	0.70	0.79	0.78
	MAE	0.030	0.044	0.098	0.063	0.044	0.064	0.088	0.100	0.036	0.104	0.120	0.111
	MBE	0.000	−0.042	−0.098	−0.063	0.009	−0.038	−0.068	−0.089	0.030	−0.095	−0.112	−0.110

was noticed, and the SP5 effectively reduced these "wet biases." *MAE* and *MBE* were also improved significantly. However, SP5 increased the *RMSE* slightly between the simulated and the observed value of the middle soil (20 cm and 40 cm); however, the *R-value* was observed to improve. Overall, the SP5 improved the simulated soil moisture effectively and reduced the "wet biases" on the permafrost regions for the shallow soil. *RMSE* of the middle soil increased slightly, but the *R-value* was improved.

4.3. Surface energy flux

Fig. 4 compares the daily mean of simulated and observed *H* at TGL

and XDT stations. An obvious overestimation of *H* at both stations was found. The experiment obtained the DSL scheme (SP4, SP5, and SP6), which effectively reduced the overestimation. Table 5 shows the statistical data for the simulated and the observed. SP6, with a mean value of 33.08 W m^{-2}, was closer to the observed mean value of 37.28 W m^{-2} at the TGL station compared to the CTL test (with a mean value of 46.45 W m^{-2}). Furthermore, the overestimation of *H* was more pronounced for the XDT station. The observed mean value was 24.60 W m^{-2}. However, the simulated mean value of the CTL test was 130.66 W m^{-2}. Although the SP6 reduced the mean value to 108.92 W m^{-2}, there was still a significant overestimation.

Fig. 5 shows the differences between the observed and simulated LE
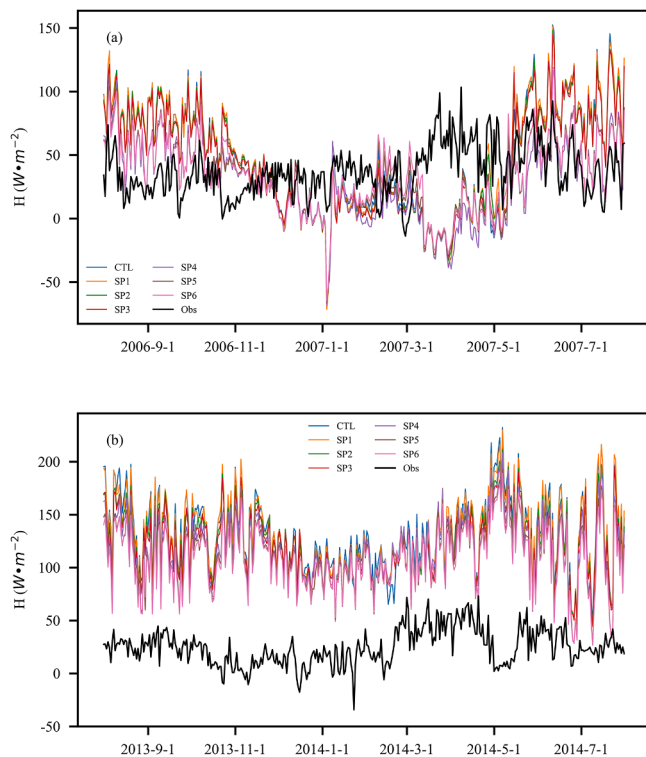
Fig. 4. Comparison of daily mean of observed and simulated H (W m^{-2}) at the (a) TGL station and (b) XDT station.

surface energy budget (Fig. 7). G_0 was positive during the thawed period, showing that the atmosphere transmits energy to the soil. Moreover, it was negative during the frozen period, indicating that the soil transmits energy to the atmosphere. CLM5.0 could describe this annual variation pattern of G_0. However, large fluctuations compared to the observed value were observed. The observed annual mean values were 1.85 W m^{-2} and 2.55 W m^{-2}, and the simulations closest to the observed values were SP6 (3.14 W m^{-2}) and SP4 (2.82 W m^{-2}), respectively.

5. Discussions

5.1. Uncertainties in the results of simulation

The annual mean daily values of soil temperature, moisture, and surface energy fluxes simulated by different schemes in CLM5.0 were analyzed. The results showed that the CLM5.0 could well simulate the soil temperature and moisture. Furthermore, it can capture the annual pattern of the surface energy fluxes in permafrost regions over the QTP; however, there still yield large errors during the frozen period.

The soil moisture is often underestimated during the frozen period and overestimated during the thawed period (Fig. 3), which is a
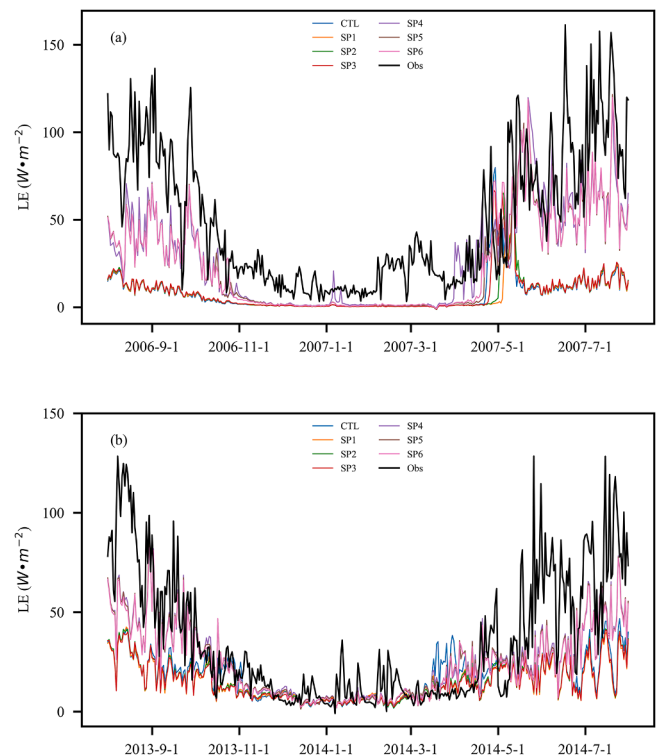
Fig. 5. Comparison of daily mean of observed and simulated LE (W m^{-2}) at the (a) TGL station and (b) XDT station.

using the different schemes at the TGL and XDT stations. An obvious increase from May to September was observed. It started declining after October. CLM5.0 can describe this pattern of LE well. However, the comparisons showed that CLM5.0 underestimated the LE. Furthermore, the observed annual mean value was 48.98 W m^{-2}, while the CTL test value was only 7.98 W m^{-2} at the TGL station. The simulated LE from the SP6 matched well with the observation, which effectively increased the annual mean value to 25.88 W m^{-2}. The XDT station also underestimated LE (Fig. 5b). The annual mean value was observed to be 26.02 W m^{-2}. Moreover, the CTL test provided the simulated value of 17.20 W m^{-2}. SP4 matched well with the observation, improving the simulated annual mean value to 25.03 W m^{-2}.

Fig. 6 shows the mean daily variability of observed and simulated R_n at the TGL and XDT stations. The simulated R_n matched well with the observed value, showing that the R_n was simulated well by the CLM5.0. The simulated mean daily values ranged between -38.55 W m^{-2} and 190.51 W m^{-2} (CTL test), and the observed values ranged between -25.94 W m^{-2} and 200.39 W m^{-2} at the TGL station. The observed annual mean values of the two stations were 78.78 W m^{-2} and 159.91 W m^{-2}, respectively. The simulated tests that were closest to the observed values were the SP6 and CTL tests at TGL and XDT stations, with mean values of 62.06 W m^{-2} and 150.97 W m^{-2}, respectively.

The ground heat flux G_0 is a comparatively small component of the

Table 5
The annual mean value of the surface energy fluxes (W m^{-2}) for simulation and observation at TGL and XDT stations.

Energy fluxes (W m^{-2})	Station	CTL	SP1	SP2	SP3	SP4	SP5	SP6	Obs
H	TGL	46.45	46.50	44.66	43.75	32.85	32.27	33.08	37.28
	XDT	130.66	129.63	123.35	121.19	116.50	111.05	108.92	24.60
LE	TGL	7.96	6.75	7.45	8.10	24.77	24.97	25.88	48.98
	XDT	17.20	14.90	15.11	14.73	25.03	24.56	23.94	26.02
R_n	TGL	57.74	56.68	55.65	55.47	60.61	60.29	62.06	78.78
	XDT	150.97	147.52	141.99	139.69	144.33	138.84	136.31	159.91
G_0	TGL	3.37	3.46	3.57	3.65	3.01	3.08	3.14	1.85
	XDT	3.12	3.01	3.53	3.78	2.82	3.24	3.46	2.55
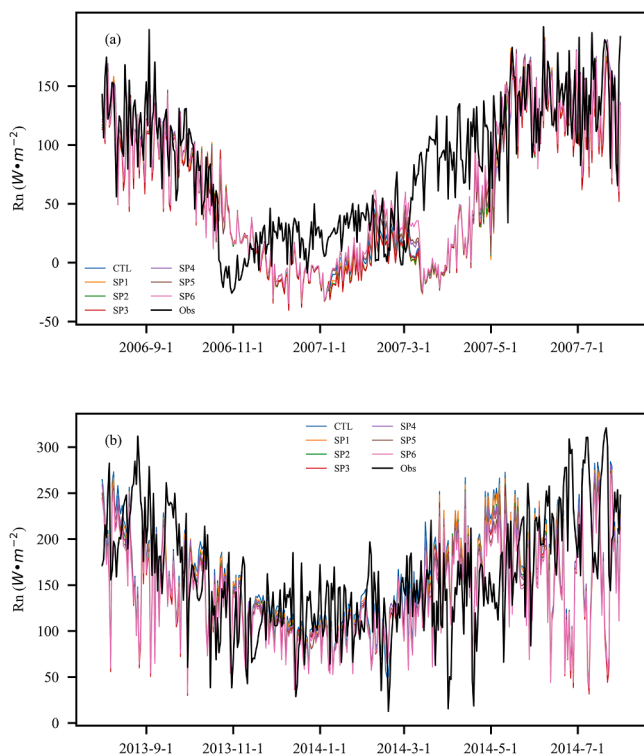
Fig. 6. Comparison of daily mean of observed and simulated R_n (W m^{-2}) at the (a) TGL station and (b) XDT station.
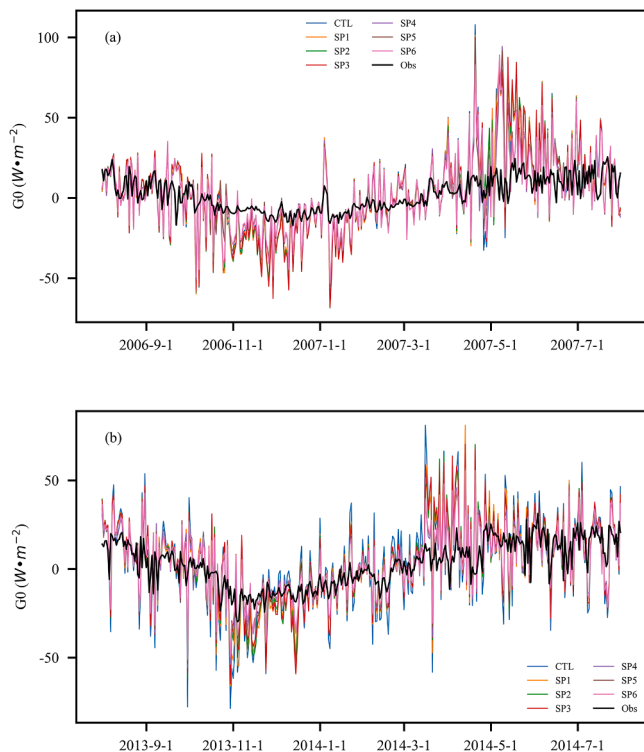
Fig. 7. Comparison of daily mean of observed and simulated G_0 (W m^{-2}) at the (a) TGL station and (b) XDT station.

commonly recognized issue in LSMs over the QTP (Deng et al., 2021; Li et al., 2020; Yang et al., 2018). The simulation effect of soil hydraulic properties is generally poor compared with the simulation performance of thermodynamic properties of soil as far as all LSMs are concerned. A

very important reason is the complexity of soil moisture, which is different from soil temperature. There is a good linear relationship on the dimensional scale for soil temperature (Li et al., 2019). However, the content of soil moisture at different depths has no obvious relationship (Yuan et al., 2020) because it is affected by several factors, such as lateral runoff and infiltration. These complex land surface processes in cold regions have not been represented well in current LSMs (Yang et al., 2009). Additionally, the main reasons for affecting the performance of the simulation are the soil organic content (Chen et al., 2012; Yang et al., 2014), soil surface resistance (Deng et al., 2021), soil stratification (Yang et al., 2009), and gravel (Yi et al., 2018).

We also noticed that soil temperature was overestimated during the thawed period, which resulted in an advanced permafrost thawing, especially at BLH and XDT sites (Fig. 2). This substantial overestimation of soil temperature at surface layer was not improved greatly by altering the scheme of thermal roughness length. This is mainly due to the complex hydrothermal process of the active layer in the permafrost region, and the simulation of soil temperature is affected by a variety of factors, such as surface energy budget, hydrothermal coupling, thermal conductivity (Li et al., 2020; Ma et al., 2022b). XDT site is located in the northernmost boundary of permafrost, which is characterized as warm permafrost type with high soil moisture content (Zhao et al., 2021). The warm permafrost has more intensive hydrothermal exchange processes compared to the cold permafrost (such as TGL site) (Ma et al., 2022b; Yao et al., 2020). Soil temperature is greatly affected by soil moisture, and the poor soil moisture simulation result is the main factor affecting the soil temperature result. Moreover, the soil temperature at top soil layer (10 cm) is well simulated at TGL, but large biases occurs in deep soil layer at 210 cm, which indicates large uncertainty in the thermal conduction along the vertical profile. The simulation error of soil temperature increases gradually with the increase of soil depth, which may be related to the imperfect consideration of freeze-thaw process in the LSMs (Li et al., 2020). During the process of soil temperature simulation, with the gradual increase of soil depth, the simulation error accumulates gradually. Therefore, the simulation error is also gradually amplified. This may be the main reason for the large error in deep soil layer.

The simulation of surface energy fluxes is more difficult compared to the soil temperature and soil moisture (Yang et al., 2009). Our study showed that H is often overestimated (Fig. 4), which is consistent with previous studies in other regions using different LSMs (Li et al., 2017; Wang et al., 2019a). This overestimation is largely due to an inappropriate thermal roughness scheme (Yang et al., 2008). A previous study showed that the thermal roughness length parameterization is very crucial for simulating the surface ground temperature and sensible heat flux (Yang et al., 2009; Zheng et al., 2014). The combination of thermal roughness and DSL schemes in this study showed the best performance in simulating H at both stations; this scheme is also very effective for simulating soil temperature (Fig. 2). The improvement of H corresponds to the soil temperature (Chen et al., 2010; Li et al., 2020; Zeng et al., 2005). The improved thermal roughness scheme effectively reduced H. More energy available for heating the ground, improving the surface soil temperature (Li et al., 2020). Furthermore, the errors in soil temperature were larger at the XDT station compared to the other stations (Fig. 2), which is consistent with the worse results of simulated H at XDT stations (Fig. 4).

Additionally, we note that the simulated value of the LE was severely underestimated (Fig. 5). Especially, the simulated value of LE was mostly 0 in the complete freezing period, which is obviously an underestimation. A major reason for this phenomenon is as follows: the unfrozen water was not very well described in the model (Hu et al., 2020), and the surface latent heat flux was significantly underestimated during the complete freezing period. Additionally, the snowfall process on the QTP was relatively complex. The snow cover quickly melts and becomes thinner due to the high wind speed and the dry climate. Therefore, the snow cover on the QTP is generally thinner (Li et al., 2020; Ma et al., 2022a). However, the snow coverage and thickness simulated by the

model were significantly different from the actual situation (Fig. 8), the simulation of surface albedo is obviously high, especially during the freezing period, which is also an important reason for the underestimate of LE during the complete freezing period. The reason for the simulation error during the thawing period may be due to the inaccurate description of soil surface resistance (Yang et al., 2009). We have also noticed that the LE was very sensitive to the DSL scheme. The underestimation improved significantly at the two stations after optimizing the DSL parameters. The LE in the model is mainly composed of vegetation evaporation, vegetation transpiration and soil evaporation. The DSL scheme is a major improvement of CLM5.0 for version 4.5 (Deng et al., 2020, 2021). Compared with the more heavily vegetated area, soil evaporation in the study area accounts for the main contribution of evapotranspiration (i.e. LE) (Miralles et al., 2011), therefore, the improvement of LE in this scheme is mainly to improve soil evaporation. For the default DSL scheme of CLM5.0, θ_{dsl0} is about 0.44 m^{3}m^{-3}, which is significantly higher than the annual soil moisture of TGL site. This will lead to overestimation of soil resistance, and thus underestimation of soil evaporation, leading to overestimation of surface soil moisture. After calibrating the DSL parameters, the overestimation of surface soil moisture was significantly improved, therefore, the soil evaporation was increased, which significantly improved the underestimation of LE.

5.2. Influence of atmospheric forcing data and soil property data

The atmospheric forcing data are essential for LSMs simulation (Guo et al., 2017). Previous studies have indicated that usage of the observed forcing data can significantly improve the simulation effect (Deng et al., 2020). This study used the observed atmospheric data at the four stations. However, the precipitation data of the LDH station experienced serious deviation due to the problem with instruments. Hence, we replaced it with precipitation data extracted from CMFD. The CMFD dataset was verified to have high simulation accuracy as forcing data in the QTP (Zhang et al., 2021b). However, a certain error still remained compared with the observed data.

Previous studies have shown that the soil properties (soil texture, soil organic matter, canopy height, etc.) directly affect surface albedo, roughness, soil thermal conductivity (Farouki, 1981; He et al., 2020; Lawrence and Slater, 2008), and several other parameters of soil hydrothermal properties, which in turn makes the changes in soil moisture, runoff, soil infiltration, and soil evapotranspiration (Dai et al., 2019). They ultimately affect the water and energy cycle between land and the atmosphere. In the LSMs, the inaccurate expression of soil properties directly affects the simulation of the soil hydrothermal properties and surface energy fluxes. This study used the observed soil properties (percent of sand and clay, soil organic matter) data in SP1 and found that the simulation effect was improved at most stations. We also noticed that the model surface was closer to the actual surface conditions of each station after modifying the soil properties. However, the simulation effect of soil temperature did not improve completely, e.g., for the TGL
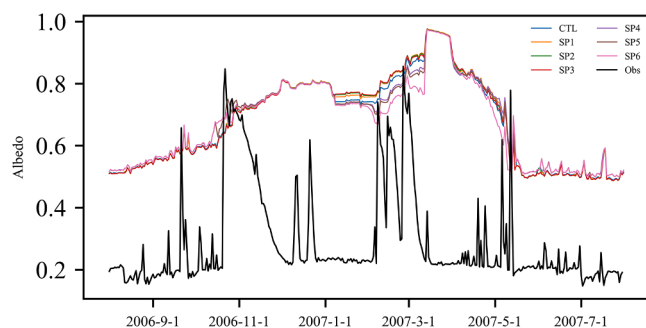
station. This phenomenon may be attributed to the inaccuracy of the soil thermal conductivity in the model (Pan et al., 2015; Yi et al., 2018), and insignificant improvement of the simulation effect was also proven in previous studies at other sites (Su et al., 2020). The gravel content is relatively high at the TGL station. However, the soil thermal conductivity in the default CLM5.0 did not consider the gravel content. The simulation effect did not significantly improve after replacing the observed soil property data.

5.3. Interactions between freeze-thaw process and surface energy fluxes

The freeze-thaw process in permafrost regions is very complex; it contains physical and chemical changes, which have an important impact on surface energy fluxes (Hu et al., 2019; Luo et al., 2014; Wani et al., 2021). Additionally, the variations of surface energy fluxes also affect the freeze-thaw process (Ma et al., 2022a). These interactions strengthen the exchange of fluxes between land and atmosphere (Chen et al., 2014). In this study, CLM5.0 captured the seasonal pattern of surface energy fluxes well after adjusting the DSL scheme, which was consistent with the variation of soil temperature and moisture. For example, In Fig. 5a, Fig. 5a shows that LE increased significantly from the end of April primarily because soil moisture started to increase rapidly during this time as the surface soil moisture began to thaw (Fig. 3a). Another period of a significant increase in LE occurred in June when precipitation began to increase, primarily due to the QTP entering the monsoon season (Gu et al., 2015; Yao et al., 2020). Furthermore, the LE began to decrease after October, mainly due to the end of the monsoon and the freezing of the soil. This was consistent with the variation of surface soil moisture. A similar pattern of LE was also obtained from other regions of the QTP (Wang et al., 2019b; Yao et al., 2011, 2020).

Additionally, the freeze-thaw process is also affected by the surface energy fluxes. Previous studies have reported that the thawing process is caused by the accumulation of surface energy fluxes (Li et al., 2011). The soil temperature increased with increasing R_n (Figs. 2 and 6). Similarly, the freezing process is also closely related to the surface energy fluxes. R_n and surface heat source are important factors affecting the freezing depth (Li et al., 2009; Ma et al., 2022a). However, compared to the thawing process, the freezing process is a bi-directional process, which is due to the combined effect of surface energy fluxes and the cold energy from the permafrost (Jiao et al., 2014; Zhao et al., 2000, 2019).

6. Conclusions and perspectives

This study investigated the soil property data, different thermal roughness length schemes, and dry surface layer schemes to evaluate the performance of soil temperature, moisture, and surface energy fluxes in CLM5.0 on the permafrost regions of the QTP. The results showed that the default scheme in CLM5.0 can well reflect the seasonal pattern of soil temperature; the simulation results of shallow soil were better than deep soil. Furthermore, an overestimation during the thawing period was noted. On the contrary, the simulation results of soil moisture were even worse, which were overestimated during the thawing period and underestimated during the freezing period. It yielded large errors while simulating surface energy fluxes in the study area.

The soil property data is important for CLM5.0. The simulation effect was improved at most stations after replacing the default soil property data with the observed values in SP1. The DSL scheme significantly improved the simulation results of soil temperature. It decreased the *RMSE* from 1.95 °C, 2.07 °C, 2.02 °C, and 2.95 °C to 1.34 °C, 1.35 °C, 1.35 °C, and 2.29 °C, respectively, at the four soil depths in TGL station. The combination of Y08 and DSL showed the best performance in shallow soil moisture. *RMSE* decreased from 0.136 m^3 m^{-3} to 0.049 m^3 m^{-3} in the XDT station; however, it slightly enhanced the errors for middle soil. The combination of B82 and DSL schemes significantly improved the simulation results of surface energy fluxes, especially for

Fig. 8. Comparison of daily mean of observed and simulated albedo at the TGL station.

latent heat flux.

Changes in one parameter also affect another due to the strong interaction between the soil hydrothermal process and surface energy budget regime. The combination of the thermal roughness scheme and DSL scheme in this study showed the best performance while simulating *H* at both stations. This scheme is also very effective in simulating soil temperature. However, the thermal roughness length and the DSL schemes are highly dependent on the condition of the underlying surfaces. Different schemes should be selected for different regions according to the real surface conditions.

Declaration of Competing Interest

The authors declare no competing interests.

Data availability

Data will be made available on request.

Acknowledgments

References

Brutsaert, W.A., 1982. Evaporation Into the Atmosphere. Springer, Netherlands.

Cao, B., Zhang, T., Wu, Q., Sheng, Y., Zhao, L., Zou, D., 2019. Brief communication: evaluation and inter-comparisons of Qinghai-Tibet Plateau permafrost maps based on a new inventory of field evidence. Cryosphere 13 (2), 511–519. https://doi.org/10.5194/tc-13-511-2019.

Chen, B., Luo, S., Lü, S., Yu, Z., Ma, D., 2014. Effects of the soil freeze-thaw process on the regional climate of the Qinghai-Tibet Plateau. Clim. Res. 59, 243–257. https://doi.org/10.3354/cr01217, 2014.

Cheng, G., Wu, T., 2007. Responses of permafrost to climate change and their environmental significance, Qinghai-Tibet Plateau. J. Geophys. Res. 112 (F2) https://doi.org/10.1029/2006jf000631.

Cheng, G., Zhao, L., Li, R., Wu, X., Sheng, Y., Hu, G., Zou, D., Jin, H., Li, X, Wu, Q., 2019. Characteristic, changes and impacts of permafrost on Qinghai-Tibet Plateau. Chin. Sci. Bull. 64 (27), 2783–2795.

Chen, Y., Yang, K., Zhou, D., Qin, J., Guo, X., 2010. Improving the Noah land surface model in arid regions with an appropriate parameterization of the thermal roughness length. J. Hydrometeorol. 11 (4), 995–1006. https://doi.org/10.1175/2010JHM1185.1.

Chen, Y., Yang, K., He, J., 2011. Improving land surface temperature modeling for dry land of China. J. Geophys. Res. 116, D20104. https://doi.org/10.1029/2011JD015921.

Chen, Y., Yang, K., Tang, W., Qin, J., Zhao, L., 2012. Parameterizing soil organic carbon's impacts on soil porosity and thermal parameters for Eastern Tibet grasslands. Sci. China Ser. D 55 (6), 1001–1011.

Chen, X., Su, Z., Ma, Y., Yang, K., Wen, J., Zhang, Y., 2013. An improvement of roughness height parameterization of the surface energy balance system (SEBS) over the Tibetan Plateau. J. Appl. Meteorol. Climatol. 52 (3), 607–622.

Dai, Y., Xin, Q., Wei, N., Zhang, Y., Shangguan, W., Yuan, H., Zhang, S., Liu, S., Lu, X., 2019. A global high-resolution data set of soilhydraulic and thermal properties forland surface modeling. Adv. Model. Earth Syst. 11 (9), 2996–3023. https://doi.org/10.1029/2019MS001784.

Deng, M., Meng, X., Lu, Y., Li, Z., Zhao, L., Hu, Z., Chen, H., Shang, L., Wang, S., Li, Q., 2021. Impact and sensitivity analysis of soil water and heat transfer parameterizations in Community Land Surface Model (CLM5.0) on the Tibetan Plateau. J. Adv. Model. Earth Syst.

Deng, M., Meng, X., Lyv, Y., Zhao, L., Li, Z., Hu, Z., Jing, H., 2020. Comparison of soil water and heat transfer modeling over the tibetan plateau using two community land

surface model (CLM) versions. J. Adv. Model. Earth Syst. 12 (10) https://doi.org/10.1029/2020MS002189.

Dickinson, R.E., Oleson, K.W., Bonan, G., Hoffman, F., Zeng, X., 2006. The community land model and its climate statistics as a component of the community climate system model. J. Clim. 9 (11), 2302–2324.

Duan, A., Wu, G., Liu, Y., Ma, Y., Zhao, P., 2012. Weather and climate effects of the Tibetan Plateau. Adv. Atmosph. Sci. 29 (5), 978–992. https://doi.org/10.1007/s00376-012-1220-y.

Farouki, O.T., 1981. The thermal-properties of soils in cold regions. Cold Reg. Sci. Technol. 5 (1), 67–75. https://doi.org/10.1016/0165-232x(81)90041-0.

Gao, Y., Xiao, X., Chen, D., Chen, F., Xu, J., Xu, Y., 2016. Quantification of the relative role of land surface processes and large scale forcing in dynamic downscaling over the Tibetan plateau. Clim. Dyn. https://doi.org/10.1007/s00382-016-3168-6.

Gu, L., Yao, J., Hu, Z., Zhao, L., 2015. Comparison of the surface energy budget between regions of seasonally frozen ground and permafrost on the Tibetan Plateau. Atmos. Res. 153, 553–564. https://doi.org/10.1016/j.atmosres.2014.10.012.

Guo, D., Wang, H., &Wang, A, 2017. Sensitivity of historical simulation of the permafrost to different atmospheric forcing data sets from 1979 to 2009. J. Geophys. Res. Atmosph. 122, 12269–12284. https://doi.org/10.1002/2017JD027477.

He, H., He, D., Jin, J., Smits, K.M., Dyck, M., Wu, Q., Si, B., Lv, J., 2020. Room for improvement: a review and evaluation of 24 soil thermal conductivity parameterization schemes commonly used in land-surface, hydrological, and soil-vegetation-atmosphere transfer models. Earth Sci. Rev. 211, 103419 https://doi.org/10.1016/j.earscirev.2020.103419.

Hu, G., Zhao, L., Li, R., Wu, X., Wu, T., Zhu, X., Pang, Q., Liu, G.Y., Du, E., Zou, D., Hao, J., Li, W., 2019. Simulation of land surface heat fluxes in permafrost regions on the Qinghai-Tibetan Plateau using CMIP5 models. Atmos. Res. 220, 155–168. https://doi.org/10.1016/j.atmosres.2019.01.006, 2019.

Hu, G., Zhao, L., Zhu, X., Wu, X., Hao, J., 2020. Review of algorithms and parameterizations to determine unfrozen water content in frozen soil. Geoderma 368.

Jiao, Y., Li, R., Zhao, L., et al., 2014. Processes of soil thawing-freezing and features of soil moisture migration in the permafrost active layer. J. Glaciol. Geocryol. 36 (2), 237−247, 2014.

Lawrence, D.M., Fisher, R.A., Koven, C.D., Oleson, K.W., Swenson, S.C., Bonan, G., Collier, N., Ghimire, B., Kampenhout, L., Kennedy, D., Kluzek, E., Lawrence, P.J., Li, F., Li, H., Lombardozzi, D., Riley, W.J., Sacks, W.J., Shi, M., Vertenstein, M., Wieder, W.R., Xu, C., Ali, A.A., Badger, A.M., Bisht, G., Broeke, M., Brunke, M.A., Burns, S.P., Buzan, J., Clark, M., Craig, A., Dahlin, K., Drewniak, B., Fisher, J.B., Flanner, M., Fox, A.M., Gentine, P., Hoffman, F., Keppel-Aleks, G., Knox, R., Kumar, S., Lenaerts, J., Leung, L.R., Lipscomb, W.H., Lu, Y., Pandey, A., Pelletier, J. D., Perket, J., Randerson, J.T., Ricciuto, D.M., Sanderson, B.M., Slater, A., Subin, Z. M., Tang, J., Thomas, R.Q., Val Martin, M., Zeng, X., 2019. The community land model version 5: description of new features, benchmarking, and impact of forcing uncertainty. J. Adv. Model. Earth Syst. 11 (12), 4245–4287. https://doi.org/10.1029/2018ms001583.

Lawrence, D.M., Slater, A.G., 2008. Incorporating organic soil into a global climate model. Clim. Dyn. 30 (2–3), 145–160. https://doi.org/10.1007/s00382-007-0278-1.

Li, C., Lu, H., Yang, K., Wright, J.S., Yu, L., Cheng, Y., Huang, X., Xu, S., 2017. Evaluation of the common land model (CoLM) from the perspective of water and energy budget simulation: towards inclusion in CMIP6. Atmosphere. 8.

Li, M., Liu, X., Shu, L., Yin, S., Wang, L., Fu, W., Ma, Y., Yang, Y., Sun, F., 2021. Variations in surface roughness of heterogeneous surfaces in the Nagqu area of the Tibetan Plateau. Hydrol. Earth Syst. Sci. 25, 2915–2930.

Li, R., Zhao, L., Ding, Y., Shen, Y., Du, E., Liu, G., 2009. The effect of global radiation budget on seasonal frozen depth in the Tibetan Plateau. J. Glaciol. Geocryol. 31 (3), 422–430.

Li, R., Zhao, L., Ding, Y., Wang, Y., Du, E., Liu, G., Xiao, Y., Sun, L., Liu, Y., Shi, W., 2011. Impact of surface energy variation on thawing processes within active layer of permafrost. J. Glaciol. Geocryol. 33 (6), 1235–1242.

Li, R., Zhao, L., Wu, T., Wang, Q., Ding, Y., Yao, J., Wu, X., Hu, G., Xiao, Y., Du, Y., Zhu, X., Qin, Y., Yang, S., Bai, R., Du, E., Liu, G., Zou, D., Qiao, Y., Shi, J., 2019. Soil thermal conductivity and its influencing factors at the Tanggula permafrost region on the Qinghai-Tibet Plateau. Agric. For. Meteorol. 264, 235–246. https://doi.org/10.1016/j.agrformet.2018.10.011.

Li, X., Wu, T., Zhu, X., Jiang, Y., Hu, G., Hao, J., Ni, J., Li, R., Qiao, Y., Yang, C., Ma, W., Wen, A., Ying, X., 2020. Improving the noah-MP model for simulating hydrothermal regime of the active layer in the permafrost regions of the Qinghai- Tibet Plateau. J. Geophys. Res. Atmos. 125 (16) https://doi.org/10.1029/2020jd032588.

Luo, S., Fang, X., Lyu, S., Zhang, Y., Chen, B., 2017. Improving CLM4.5 simulations of land–atmosphere exchange during freeze–thaw processes on the Tibetan Plateau. J. Meteorol. Res. 31 (5), 916–930. https://doi.org/10.1007/s13351-017-6063-0.

Luo, Q., Wen, J., Hu, Z.Y., Lu, Y.Q., Yang, X.Y., 2020. Parameter sensitivities of the community land model at two alpine sites in the three-river source region. J. Meteorolog. Res. 34 (4), 851–864. https://doi.org/10.1007/s13351-020-9205-8.

Luo, D., Jin, H., Lu, L., Wu, Q., 2014. Spatiotemporal characteristics of freezing and thawing of the active layer in the source areas of the Yellow River (SAYR). Chin. Sci. Bull. 59 (24), 3034–3045.

Ma, J.J., 2022a. The surface energy budget and its impact on the freeze-thaw processes of active layer in the permafrost regions of the Qinghai-Tibetan Plateau. Adv. Atmos. Sci. 39 (1), 189–200.

Ma, J.J., 2022b. Evaluation and spatio-temporal analysis of surface energy flux in permafrost regions over the Qinghai-Tibet Plateau and Arctic using CMIP6 models. Int. J. Digit. Earth 15, 1, 1948-1966.

Miralles, D.G., de Jeu, R.A.M., Gash, J.H., Holmes, T.R.H., Dolman, A.J., 2011. Magnitude and variability of land evaporation and its components at the global

scale. Hydrol. Earth Syst. Sci. 15, 967–981. https://doi.org/10.5194/hess-15-967-2011.

Mu, C., Abbott, B.W., Norris, A.J., Mu, M., Fan, C., Chen, X.u., Jia, L., Yang, R., Zhang, T., Wang, K., Peng, X., Wu, Q., Guggenberger, G., Wu, X., 2020. The status and stability of permafrost carbon on the Tibetan Plateau. Earth Sci. Rev. 211, 103433 https://doi.org/10.1016/j.earscirev.2020.103433.

Ma, Y., Fan, S., Ishikawa, H., Tsukamoto, O., Yao, T., Koike, T., 2004. Diurnal and inter-monthly variation of land surface heat fluxes over the central Tibetan Plateau area. Theor. Appl. Climatol. 80, 259–273. https://doi.org/10.1007/s00704-004-0104-1.

Ma, Y., Kang, S., Zhu, L., Xu, B., Tian, L., Yao, T., 2008. Tibetan observation and research platform (TORP): atmosphere–land interaction over a heterogeneous landscape. Bull. Amer. Meteor. Soc. 8, 1487–1492.

Pan, Y., Lyu, S., Li, S., Gao, Y., Meng, X., Ao, Y., Wang, S., 2015. Simulating the role of gravel in freeze–thaw process on the Qinghai-Tibet Plateau. Theor. Appl. Clim. 127 (3–4), 1011–1022. https://doi.org/10.1007/s00704-015-1684-7.

Su, Y., Zhang, Yu., Song, M., et al., 2020. Evaluation of simulated performance of CLM4. 5 in alpine meadow over the Qinghai-Xizang plateau based on measured soil properties. Plateau Meteorol. 39 (6), 1295–1308. https://doi.org/10.7522/j.issn.1000-0534.2019.000136.

Swenson, S.C., Lawrence, D.M., 2014. Assessing a dry surface layer-based soil resistance parameterization for the community land model using GRACE and FLUXNET-MTE data. J. Geophys. Res. Atmos. 119 (17), 10299–10312. https://doi.org/10.1002/2014JD022314.

Wang, S., Ma, Y., 2019a. On the simulation of sensible heat flux over the Tibetan Plateau using different thermal roughness length parameterization schemes. Theor. Appl. Climatol. 137, 1883–1893.

Wani, J.M., Thayyen, R.J., Ojha, C.S.P., Gruber, S., 2021. The surface energy balance in a cold and arid permafrost environment, Ladakh, Himalayas, India. Cryosphere 15, 2273–2293.

Wang, J., Luo, S., Li, Z., Wang, S., Li, Z., 2019b. The freeze-thaw process and the surface energy budget of the seasonally frozen ground in the source region of the Yellow River. Theor. Appl. Climatol. 138, 1631–1646. https://doi.org/10.1007/s00704-019-02917-6.

Wu, D., Hu, Z., Fu, C., Wang, S., Fan, W., 2022. A simulation study on radiation budget and water-heat Ex- change over alpine grassland based on CLM4. 5. Plateau Meteorol. 41 (1), 107–121.

Wu, G.X., Liu, Y., He, B., Bao, Q., Duan, A., Jin, F.F., 2012. Thermal controls on the Asian summer monsoon. Sci. Rep. 2 (404) https://doi.org/10.1038/srep00404.

Xin, Y., Chen, F., Zhao, P., Barlage, M., Blanken, P., Chen, Y., Chen, B., Wang, Y., 2018. Surface energy balance closure at ten sites over the Tibetan plateau. Agric. For. Meteorol. 259, 317–328.

Yang, F., Zhang, G., Yang, J., Li, D., Zhao, Y., Liu, F., et al., 2014. Organic matter controls of soil water retention in an alpine grassland and its significance for hydrological processes. J. Hydrol. 519, 3086–3093. https://doi.org/10.1016/j.jhydrol.2014.10.054 (Amst).

Yang, K., Chen, Y., Qin, J., 2009. Some practical notes on the land surface modeling in the Tibetan Plateau. Hydrol. Earth Sci.s 13 (5), 687–701. https://doi.org/10.5194/hess-13-687-2009.

Yang, K., Wang, C., Li, S., 2018. Improved simulation of frozen-thawing process in land surface model (CLM4.5). J. Geophys. Res. Atmos. 123 (23) https://doi.org/10.1029/2017jd028260.

Yang, K., Koike, T., Ishikawa, H., Kim, J., Li, X., Liu, H.Z., Liu, S.M., Ma, Y.M., Wang, J. M., 2008. Turbulent flux transfer over bare-soil surfaces: characteristics and parameterization. J. Appl. Meteorol. Climatol. 47 (1), 276–290. https://doi.org/10.1175/2007jamc1547.1.

Yang, K., Koike, T., Yang, D., 2003. Surface flux parameterization in the Tibetan Plateau. Boundary Layer Meteorol. 106 (2), 245–262. https://doi.org/10.1023/A:1021152407334.

Yao, J., Zhao, L., Gu, L., Qiao, Y., Jiao, K., 2011. The surface energy budget in the permafrost region of the Tibetan Plateau. Atmos. Res. 102 (4), 394–407. https://doi.org/10.1016/j.atmosres.2011.09.001.

Yao, J., 2020. Estimation of surface energy fluxes in the permafrost region of the Tibetan Plateau based on *in situ* measurements and the surface energy balance system model. Int. J. Climatol. 40 (13), 5783–5800. https://doi.org/10.1002/joc.6551.

Yao, T., Xue, Y., Chen, D., Chen, F., Thompson, L., Cui, P., Koike, T., Lau, W.K.M., Lettenmaier, D., Mosbrugger, V., Zhang, R., Xu, B., Dozier, J., Gillespie, T., Gu, Y., Kang, S., Piao, S., Sugimoto, S., Ueno, K., Wang, L., Wang, W., Zhang, F., Sheng, Y., Guo, W., AilikunYang, X., Ma, Y., Shen, S.S.P., Su, Z., Chen, F., Liang, S., Liu, Y., Singh, V.P., Yang, K., Yang, D., Zhao, X., Qian, Y., Zhang, Y., Li, Q., 2019. Recent third pole's rapid warming accompanies cryospheric melt and water cycle intensification and interactions between Monsoon and environment: multidisciplinary approach with observations, modeling, and analysis. Bull. Am. Meteorol. Soc. 100 (3), 423–444. https://doi.org/10.1175/bams-D-17-0057.1.

Yi, S., He, Y., Guo, X., Chen, J., Wu, Q., Qin, Y., Ding, Y., 2018. The physical properties of coarse-fragment soils and their effects on permafrost dynamics: a case study on the central Qinghai-Tibetan Plateau. Cryosphere 12 (9), 3067–3083. https://doi.org/10.5194/tc-12-3067-2018.

Yuan, L., Zhao, L., Li, R., Hu, G., Ma, L., 2020. Spatiotemporal characteristics of hydrothermal processes of the active layer on the central and northern Qinghai-Tibet plateau. Sci. Total Environ. 712, 136392.

Zheng, D., Rogier, V.D.V., Su, Z., et al., 2014. Assessment of roughness length schemes implemented within the Noah Land Surface Model for high-altitude regions. J. Hydrometeorol. 15 (5), 921–937.

Zeng, X., Dickinson, R., 1998. Effect of surface sublayer on surface skin temperature and fluxes. J. Clim. 11, 537–550. https://doi.org/10.1175/1520-0442(1998)011<0537:EOSSOS>2.0.CO;2.

Zeng, X., Dickinson, R., Barlage, M., Dai, Y., Wang, G., Oleson, K., 2005. Treatment of under canopy turbulence in land models. J. Clim. 18 (23), 5086–5094. https://doi.org/10.1175/Jcli3595.1.

Zeng, X., Wang, Z., Wang, A., 2012. Surface skin temperature and the interplay between sensible and ground heat fluxes over arid regions. J. Hydrometeorol. 13 (4), 1359–1370. https://doi.org/10.1175/JHM-D-11-0117.1.

Zhang, G., Nan, Z., Zhao, L., Liang, Y., Cheng, G., 2021b. Qinghai-Tibet Plateau wetting reduces permafrost thermal responses to climate warming. Earth Planet. Sci. Lett. 562, 116858, 2021.

Zhao, L., Cheng, G., Li, S., Zhao, X., Wang, S., 2000. Thawing and freezing processes of active layer in Wudaoliang region of Tibetan Plateau. Chin. Sci. Bull. 45 (23), 2181–2187.

Zhao, L., Zou, D., Hu, G., Wu, T., Du, E., Liu, G., Xiao, Y., Li, R., Pang, Q., Qiao, Y., Wu, X., Sun, Z., Xing, Z., Sheng, Y., Zhao, Y., Shi, J., Xie, C., Wang, L., Wang, C., Cheng, G., 2021. A synthesis dataset of permafrost thermal state for the Qinghai–Tibet (Xizang) Plateau, China. Earth Syst. Sci. Data 13, 4207–4218.

Zhao, L., Zou, D., Hu, G., Du, E., Pang, Q., Xiao, Y., Li, R., Sheng, Y., Wu, X., Sun, Z., Wang, L., Wang, C., Ma, L., Zhou, H., Liu, S., 2020. Changing climate and the permafrost environment on the Qinghai-Tibet (Xizang) plateau. Permafrost and Periglacial Processes 31 (3), 396–405.

Zhang, J., Wu, L., Dong, W., 2011. Land-atmosphere coupling and summer climate variability over East Asia. J. Geophys. Res. 116.

Zhang, G., Chen, F., Gan, Y., 2016. Assessing uncertainties in the Noah-MP ensemble simulations of a cropland site during the Tibet joint International cooperation program field campaign. J. Geophys. Res. Atmos. 121 https://doi.org/10.1002/2016JD024928.

Zhang, X., Chen, L., Ma, Z., Gao, Y., 2021a. Assessment of surface exchange coefficients in the Noah-MP land surface model for different land-cover types in China. Int. J. Climatol. 41, 2638–2659.

Zou, D., Zhao, L., Sheng, Y., Chen, J., Hu, G., Wu, T., Wu, J., Xie, C., Wu, X., Pang, Q., Wang, W., Du, E., Li, W., Liu, G., Li, J., Qin, Y., Qiao, Y., Wang, Z., Shi, J., Cheng, G., 2017. A new map of permafrost distribution on the Tibetan Plateau. Cryosphere 11 (6), 2527–2542. https://doi.org/10.5194/tc-11-2527-2017.